JACS
JOURNAL OF THE AMERICAN CHEMICAL SOCIETY
Article
pubs.acs.org/JACS

Photophysical Properties of *cis*-Mo_2 Quadruply Bonded Complexes and Observation of Photoinduced Electron Transfer to Titanium Dioxide

Samantha E. Brown-Xu, Malcolm H. Chisholm,* Christopher B. Durr, Terry L. Gustafson,* and Thomas F. Spilker

Department of Chemistry and Biochemistry, The Ohio State University, Columbus, Ohio 43210, United States

Supporting Information

ABSTRACT: The compounds *cis*-$Mo_2(DAniF)_2(L)_2$ have been prepared, where DAniF = (*N*,*N*′)-*p*-dianisyl formamidinate and L = thienyl-2-carboxylate (Th), 2,2′-bithienyl-5-carboxylate (BTh), and 2,2′:5′,5″-terthienyl-5-carboxylate (TTh). The compounds have been characterized by proton nuclear magnetic resonance (^{1}H NMR), ultraviolet−visible (UV−vis) absorption and emission, differential pulse voltammetry, and time-resolved transient absorption and infrared (IR) spectroscopy. An X-ray crystal structure was obtained for the thienyl complex. The related salt $[^nBu_4N]_2[Mo_2(DAniF)_2(TTh{-}CO_2)_2]$, where TTh−$CO_2$ = 2,2′:5′,2″-terthienyl-5,5″-dicarboxylate, has also been prepared and employed in the attachment of the complex to TiO_2 nanoparticles. The latter have been characterized by ground-state Fourier transform infrared spectroscopy (FTIR) and femtosecond time-resolved IR spectroscopy. The time-resolved data provide evidence for sub-picosecond charge injection from the Mo_2 center to the semiconducting oxide particle.

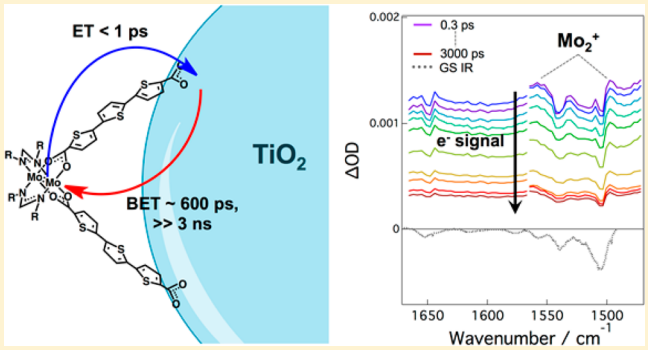

INTRODUCTION

Photon harvesting for either the synthesis of fuels or the production of electricity represents attractive goals toward the solution of the world's ever-increasing demands in energy consumption. Grätzel's pioneering work with dye-sensitized solar cells (DSSCs) employing ruthenium bipyridyl complexes attached to titanium dioxide was transformative in demonstrating the potential for construction of related devices based on organic−inorganic hybrid materials for photovoltaic applications.[1−4] Numerous systems continue to be studied to improve device characteristics[5−11] as well as understand the underlying electron-transfer processes.[12−18]

We have recently been examining the photophysical properties of carboxylates bound to dinuclear metal centers containing MM quadruple bonds (MM = Mo_2, MoW, or W_2).[19−23] These compounds have intense metal−to−ligand charge-transfer absorptions that can be tuned by the selection of MM and the attendant carboxylates to span the region from 400 to 1100 nm. Moreover, the ^{1}MLCT states are relatively long-lived, $\tau \sim 1{-}20$ ps, prior to conversion to the triplet state T_1, which may be ^{3}MLCT or ^{3}MM$\delta\delta$*. We were thus attracted to the notion that the dinuclear unit could be used as a photosensitizer and modified to mimic the well-known Grätzel dyes.

To facilitate binding to a metal oxide surface, a *cis* ligand geometry is more suitable and can be achieved using amidinate-type ancillary ligands. These NCN ligands are less kinetically labile than their carboxylate counterparts and can be used to produce ligand substitution patterns that are otherwise difficult to obtain.[24−26] The structures of the Mo_2 dicarboxylate compound studied in this work and the typical N3 dye are compared in Figure 1. For the N3 dye, photoinduced charge transfer places the electron on a dicarboxybipyridine (dcbpy)

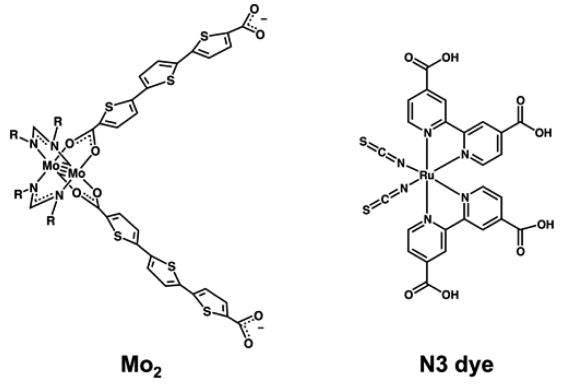

Figure 1. *cis*-Mo_2 terthienyl dicarboxylate complex compared to the Ru(II) N3 dye.

Received: May 17, 2014
Published: July 21, 2014

   dx.doi.org/10.1021/ja504944d | J. Am. Chem. Soc. 2014, 136, 11428−11435

ligand with the hole spread over the ruthenium(III) center and the NCS ligands, which aids in reduction of the oxidized metal center by I^-.[2] In the *cis*-formamidinate dimolybdenum complexes, there is a similar dipole moment and photoexcitation places an electron on the carboxylate ligand, leaving a hole on the Mo_2 center. The Mo_2 δ orbital mixes significantly with the formamidinate ligands, which could similarly facilitate reduction of the photooxidized Mo_2 center. We describe herein our initial work motivated by these considerations.

RESULTS AND DISCUSSION

Synthesis. The neutral compounds *cis*-$Mo_2(DAniF)_2(L)_2$, where DAniF = *N*,*N*′-*p*-dianisyl formamidinate and L = thienyl-2-carboxylate (Th), 2,2′-bithienyl-5-carboxylate (BTh), and 2,2′:5′,5″-terthienyl-5-carboxylate (TTh), were prepared according to the salt metathesis reaction shown in Scheme 1.

Scheme 1. Synthesis of Complexes of the Type *cis*-$Mo_2(DAniF)_2(L)_2$

$$[Mo_2(DAniF)_2(CH_3CN)_6^{2+}][BF_4^-]_2 + 2[^nBu_4N^+][L^-] \xrightarrow[\text{RT}]{CH_3CN,\ 3\text{-}5\ d} Mo_2(DAniF)_2(L)_2 + 2[^nBu_4N^+][BF_4^-]$$

The reactions were stirred for 3−5 days and resulted in the formation of a microcrystalline precipitate, which was orange, dark red, and purple for L = Th, BTh, and TTh, respectively. The solid was recovered by centrifugation and washed with CH_3CN and Et_2O to remove impurities. The complexes are soluble primarily in tetrahydrofuran (THF) and dichloromethane (DCM). Recrystallization was performed in a mixture of hexanes in THF, and the purified complexes were characterized by proton nuclear magnetic resonance (^1H NMR), matrix-assisted laser desorption ionization−time of flight (MALDI−TOF), ultraviolet−visible (UV−vis) absorption and emission, Fourier transform infrared spectroscopy (FTIR), and differential pulse voltammetry. The anionic dimolybdenum complex *cis*-$Mo_2(DAniF)_2(TTh{-}CO_2)_2$, where TTh−$CO_2$ = 2,2′:5′,2″-terthienyl-5,5″-dicarboxylate, was prepared in a similar manner; however, in this case, the dicarboxylate salt $[^nBu_4N]_2[TTh{-}CO_2]$ was employed. The structures of the complexes are shown in Figure 2.

Attachment of this dianionic complex to TiO_2 was achieved by adding a suspension of 25 nm particles to a solution of complex **4** prepared *in situ*. TiO_2 immediately took on a purple color, indicating adsorption to the surface. Successive washing with THF eventually resulted in a clear supernatant, indicating successful removal of any remaining unbound complex, while the solid remained colored. It was also observed that the sensitized particles could be made in a complementary way. First, the dianionic ligand $[^nBu_4N]_2[TTh{-}CO_2]$ was added to a TiO_2 suspension, causing the particles to become yellow in color. The carboxylated nanoparticles were washed and isolated, then resuspended in THF, and allowed to react in solution with the dimolybdenum dication $Mo_2(DAniF)_2(CH_3CN)_6^{2+}$. This stepwise adsorption procedure also resulted in a purple product and should enable dications with other ancillary ligands to be used in future studies. In both preparations, surface-bound TiO_2 was stored in THF solutions under an inert atmosphere.

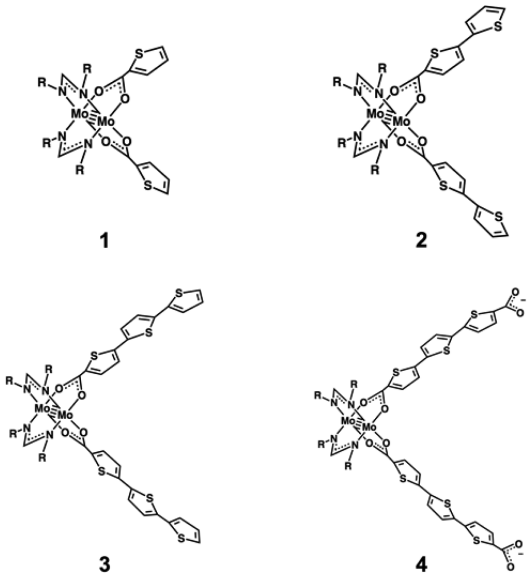

Figure 2. Structures of *cis*-$Mo_2(DAniF)_2(Th)_2$ (**1**), *cis*-$Mo_2(DAniF)_2(BTh)_2$ (**2**), *cis*-$Mo_2(DAniF)_2(TTh)_2$ (**3**), and *cis*-$Mo_2(DAniF)_2(TTh{-}CO_2)_2$ (**4**).

Single-Crystal X-ray Structure. Crystals of *cis*-$Mo_2(DAniF)_2(Th)_2$ (**1**) were grown by the slow diffusion of hexanes into a solution of the complex in THF. The resultant orange crystals were suitable for single-crystal X-ray crystallography. A summary of the crystal data is given in Table 1, and full details are given in the Supporting Information. An Oak Ridge thermal ellipsoid plot (ORTEP) drawing of the crystal structure revealing the *cis* ligand geometry is given in Figure 3. The molecule has a crystallographically imposed C_2 rotational axis bisecting the two sets of *cis* ligands and passing between the molybdenum atoms. The mutually *cis* geometry is expected on

Table 1. Data Collection Parameters for Compound 1

compound	1
chemical formula	$C_{40}H_{36}Mo_2N_4O_8S_2$
formula weight	956.73
temperature (K)	180 (2)
space group	orthorhombic, *Pbcn*
a (Å)	18.9078 (2)
b (Å)	9.9378 (1)
c (Å)	21.7123 (2)
V (Å^3)	4079.78 (7)
Z	4
D_{calcd} (Mg/m^3)	1.558
crystal size (mm)	0.19 × 0.19 × 0.12
θ range for data collection	2.15−27.49°
μ (Mo Kα) (mm^{-1})	0.773
reflections collected	46377
unique reflections	4672 [*R*(int) = 0.047]
completeness to θ_{max} (%)	99.7
data/restraints/parameters	4672/0/268
*R*1[a] (%) (all data)	2.89 (4.92)
*wR*2[b] (%) (all data)	6.51 (7.13)
goodness-of-fit on F^2	1.022
largest diff. peak and hole (e Å^{-3})	0.629 and −0.316

[a] $R1 = \sum||F_o| - |F_c||/\sum|F_o| \times 100$. [b] $wR2 = [\sum w(F_o^2 - F_c^2)^2/\sum(w|F_o|^2)^2]^{1/2} \times 100$.

dx.doi.org/10.1021/ja504944d | J. Am. Chem. Soc. 2014, 136, 11428−11435

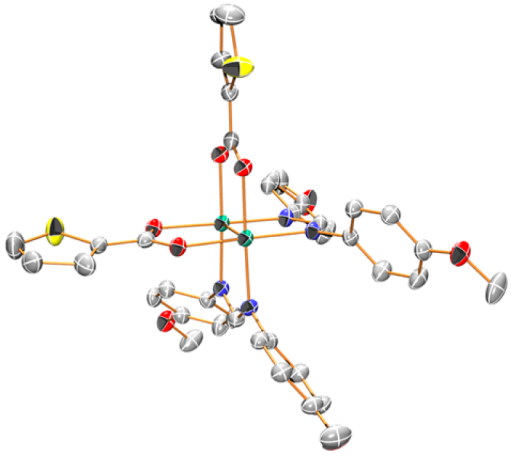

Figure 3. Single-crystal X-ray structure of *cis*-$Mo_2(DAniF)_2(Th)_2$. Thermal ellipsoids are drawn at the 50% level. Hydrogens have been removed for clarity. Green, molybdenum; yellow, sulfur; blue, nitrogen; scarlet, oxygen; and gray, carbon. Mo–Mo, 2.095 Å; Mo–N, 2.101 Å; Mo–O, 2.127 Å; N–C–N, 117.95°; and O–C–O, 122.95°.

the basis of the *trans* influence of N > O. The central $Mo_2N_2O_2$ core appears as expected for a Mo_2 quadruply bonded center, with N–Mo–O bond angles near 90° and a Mo–Mo distance of 2.095 Å.[27] The thiophene rings are almost planar to the carboxylate group with a torsion angle of 7.1°, implying extended L π–Mo_2 δ conjugation. Because of the low energy barrier of rotation along the carboxylate-to-ring C–C bond, the thiophenes were slightly disordered and were modeled in two locations. Other relevant metric parameters are given in the caption of Figure 3.

Electronic Absorption and Emission. The electronic absorption spectra of the three neutral compounds are compared in Figure 4. The lowest energy transition in each

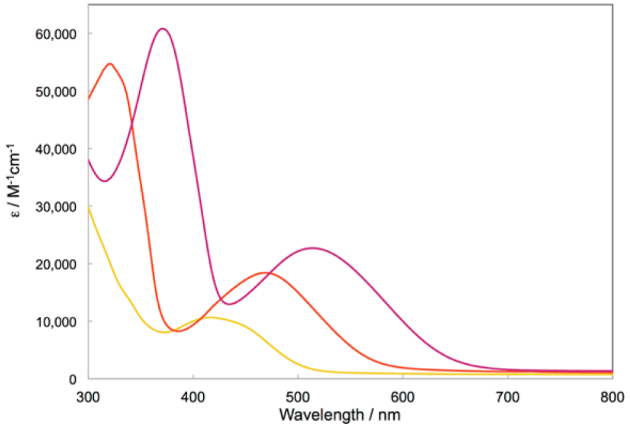

Figure 4. Electronic absorption spectra of *cis*-$Mo_2(DAniF)_2(L)_2$ complexes **1** (orange), **2** (red), and **3** (purple) collected in THF at room temperature.

case occurs in the visible region and is due to metal–to–ligand charge transfer (MLCT) to the carboxylate ligands. With increasing numbers of thiophene rings, the transitions grow in intensity and move to lower energy, corresponding to the yellow to purple color shift observed. The λ_{max} for the ^{1}MLCT transitions are 418 nm for complex **1**, 470 nm for complex **2**, and 515 nm for complex **3**. The ligand $\pi\pi^*$ transitions at higher energy show a similar red shift with increasing ligand conjugation and match closely the absorptions of the free ligands. A MLCT transition to the formamidinate ligands is expected at higher energy, although it is likely hidden under the more intense ligand-based absorptions.

Steady-state emission spectra have been obtained for the neutral complexes by irradiating into their ^{1}MLCT bands (Figure 5). All of the compounds show weak singlet emission

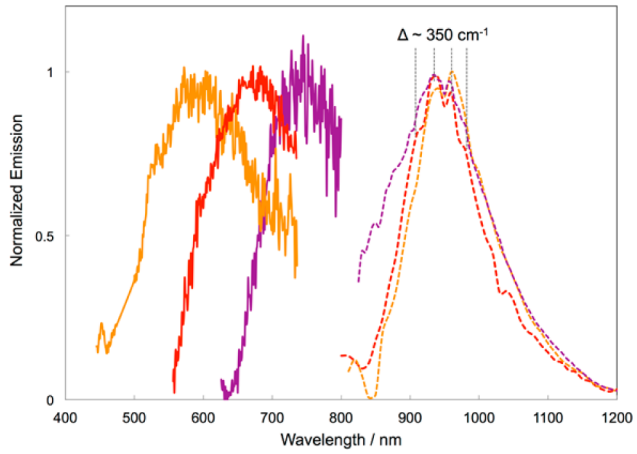

Figure 5. Normalized fluorescence spectra collected in THF at room temperature (solid lines) and phosphorescence spectra collected in 2-MeTHF at 77 K (dashed lines) for *cis*-$Mo_2(DAniF)_2(L)_2$ complexes **1** (orange), **2** (red), and **3** (purple).

from the ^{1}MLCT state with roughly a 6000 cm^{-1} Stokes shift. The complexes also show room temperature phosphorescence from the T_1 state at 950 nm in all cases. Upon cooling to 77 K, the bands sharpen and vibronic features spaced by approximately 350 cm^{-1} become evident. The nearly identical emission energy and vibronic features that correspond to ν(MoMo) are characteristic of phosphorescence from a ^{3}MoMo$\delta\delta^*$ state, which lies around 11 000 cm^{-1} above the ground state in these complexes.[23]

Electronic Structure Calculations. Calculations employing density functional theory (DFT) were performed on model compounds of complexes **1**, **2**, and **3**, where the DAniF ligand was abbreviated to HNC(H)NH to reduce computational time. A frontier molecular orbital energy level diagram is shown in Figure 6, and GaussView[28] representations of relevant orbitals are shown for complex **2**. The highest occupied molecular orbital (HOMO) is principally a Mo_2 δ orbital with some ligand mixing, largely with the filled NCN π orbitals. The lowest unoccupied molecular orbital (LUMO) and LUMO + 1 are in- and out-of-phase thienyl carboxylate π^* combinations, of which the LUMO + 1 has a small contribution of Mo_2 δ, whereas the LUMO has no Mo_2 δ component. This bonding situation is somewhat analogous to bonding in a mononuclear *cis*-$M_{d\pi}(CO)_2$ complex.

Increasing numbers of thiophene rings cause the LUMO and LUMO + 1 to move to lower energy, and the separation of these orbitals increases from 0.1 to 0.2 eV as the interaction with the Mo_2 δ orbital increases. In all cases, the Mo_2 δ^* orbital is found at higher energy. Below the Mo_2 δ lies a filled NCN orbital, which causes the HOMO to be raised >0.5 eV relative to tetracarboxylate complexes.[29]

Time-dependent DFT (TD-DFT) calculations were also performed, and two MLCT transitions, HOMO → LUMO and

dx.doi.org/10.1021/ja504944d | J. Am. Chem. Soc. 2014, 136, 11428–11435

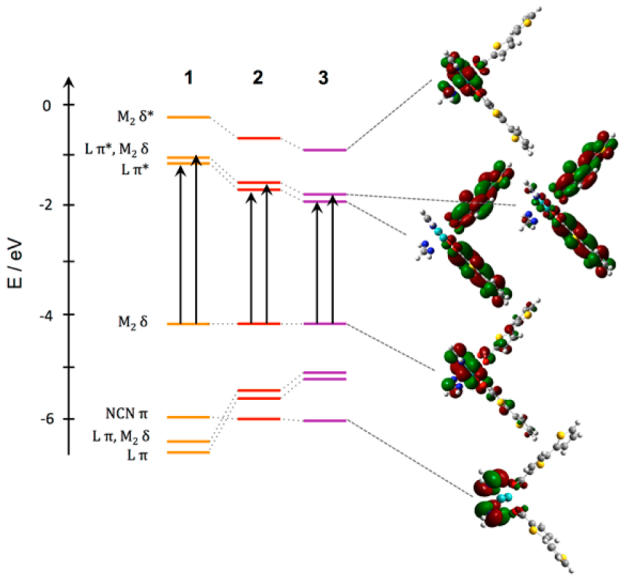

Figure 6. Frontier orbital energy diagram for complexes **1**−**3**. GaussView 5.0.8[28] isosurface contour plots for complex **2** are shown.

HOMO → LUMO + 1, are predicted. This is as opposed to trans-substituted compounds with D_{2h} symmetry, in which only the Mo δ to in-phase ligand π^* transition is allowed. The reduced symmetry of the *cis* complexes enables both transitions to occur, although the calculated energy separation is only 0.2 eV and the bands are not resolved experimentally.

Electrochemistry. Oxidation and reduction potential values determined from differential pulse voltammetry are summarized in Table 2 for the four molecular complexes. Also listed are

Table 2. Oxidation, Reduction, E_{0-0}, and Excited-State Reduction Potentials for *cis*-$Mo_2(DAniF)_2(L)_2$ Complexes 1−4

	E_{ox}[a] (V)	E_{red}[a] (V)	E_{0-0}[b] (eV)	$E(Mo_2^+/*Mo_2)$[c] (V)
1	−0.31	−2.84	2.53	−2.84
2	−0.27	−2.53	2.19	−2.46
3	−0.27	−2.24 and −2.58	1.90	−2.17
4	−0.28	−2.27 and −2.57	1.88	−2.16

[a]Values obtained from differential pulse voltammetry in THF solution and referenced to Fc/Fc^+. [b]Determined from intersection of absorption and fluorescence spectra. [c]Calculated from $E(M^+/*M) = E_{ox} - E_{0-0}$.

the zero−zero transition energies, E_{0-0}, determined from the intersection of the absorption and fluorescence bands and the calculated excited-state oxidation potentials, $E(Mo_2^+/*Mo_2)$. In all cases, a reversible oxidation is observed around −0.3 V versus the ferrocene−ferrocenium couple because of the removal of an electron from the Mo_2 δ orbital. The first reduction potential corresponds to placement of an electron in the ligand π^* orbital and becomes less negative as ligand conjugation increases. Reduction for monothienyl complex **1** is quasi-reversible and occurs at −2.84 V. This potential shifts to −2.53 V for complex **2** and −2.24 V for complex **3**, and the process becomes irreversible. Oxidation and reduction of complex **4** occur at very similar energies to the uncarboxylated analogue **3**, and a second ligand reduction is observed for both terthiophene complexes within the solvent window.

Characterization of Mo_2@TiO_2. The electronic absorption spectra for the salt **4** and for the complex bound to TiO_2, abbreviated as Mo_2@TiO_2, are compared in Figure 7. The

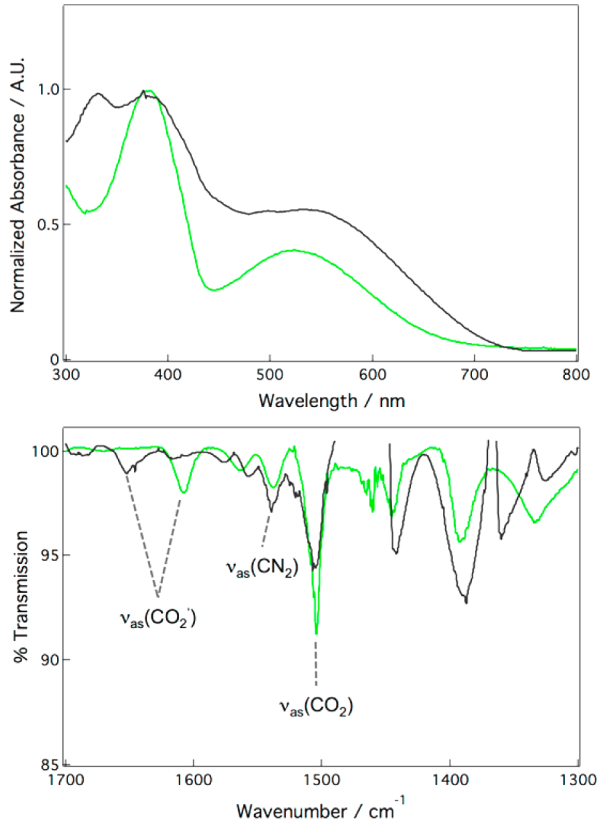

Figure 7. (Top) Normalized electronic absorption spectra of complex **4** (green) and Mo_2@TiO_2 (black) in THF at room temperature. (Bottom) FTIR spectra of complex **4** (green) and Mo_2@TiO_2 (black) in THF at room temperature. Relevant vibrations are highlighted.

spectrum of complex **4** is very similar to its neutral analogue, as might be expected. The strong absorption at λ_{max} = 522 nm is only marginally red-shifted, and the complex is also a deep purple color. When adsorbed to the surface of TiO_2, the features are significantly broadened and the MLCT maximum shifts around 15 nm to lower energy. This indicates some degree of coupling between the carboxylate and the TiO_2 conduction band.

The infrared (IR) spectra for complex **4** and Mo_2@TiO_2 are also compared in Figure 7, and relevant vibrational energies are given in Table 3. Significant similarities are seen in the vibrational modes associated with the formamidinate and carboxylate groups attached to the Mo_2 center. Specifically, the asymmetric CN_2 and CO_2 stretches occur at 1540 and 1505

Table 3. Vibrational Energies (cm^{-1}) of CO_2', CN_2, and CO_2 Groups in Compound 4 and Mo_2@TiO_2

vibration	4	Mo_2@TiO_2
$\nu_{as}(CO_2')$	1610	1650
$\nu_{as}(CN_2)$	1540	1540
$\nu_{as}(CO_2)$	1505	1505
$\nu_s(CN_2)$	1445	1442
$\nu_s(CO_2)$	1390	1390
$\nu_s(CO_2')$	1330	1365

dx.doi.org/10.1021/ja504944d | J. Am. Chem. Soc. 2014, 136, 11428−11435

cm^{-1}, respectively, and the corresponding symmetric stretches occur at 1445 and 1390 cm^{-1} These vibrations are consistent with other mixed carboxylate−formamidinate Mo_2 complexes and are not expected to be affected by adsorption. However, the modes associated with the terminal carboxylate group, designated CO_2', do undergo a change when bound to TiO_2. In the free complex, $\nu_{as}(CO_2')$ and $\nu_s(CO_2')$ are observed at 1610 and 1330 cm^{-1}, respectively. Upon formation of Mo_2@TiO_2, the IR spectrum becomes more complex but modes for the formerly free carboxylate are shifted to higher energy, $\nu_{as}(CO_2')$ to 1650 cm^{-1} and $\nu_s(CO_2')$ to 1365 cm^{-1}. This assignment does not rule out the possibility that inhomogeneous surface binding may produce CO_2' vibrations with different energies, as elaborated below.

The carboxylate IR modes of ruthenium(II) dcbpy-based dyes have been extensively studied, with the aim of establishing the mode of attachment to the TiO_2 surface.[30−33] The three principal modes of binding are shown in Figure 8 and, in a

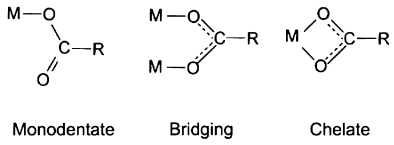

Figure 8. Possible binding modes of a carboxylate group on a metal oxide surface.

limiting description, can be referred to as monodentate η^1-O_2C, bridging Ti−OCO−Ti similar to that in $M_2(O_2CR)_4$ compounds, and chelating Ti−O_2C. For a monodentate-bound ligand, a higher energy ν(C═O) band is expected for the uncoordinated ketonic oxygen with a larger energy separation between this vibration and the symmetric-type $\nu(CO_2)$ stretch. In some cases, the bridging and chelate modes have been differentiated by measuring the energy difference (Δ) between the symmetric and asymmetric CO_2 vibrations in the free carboxylate anion and the TiO_2-supported complex.[30] When the observed separation is similar to the free anion, this has been taken as evidence of binding through a bridging mode. If the difference is notably smaller than the free anion, chelate binding is predicted. The Δ values obtained from the IR spectra are 280 cm^{-1} when unbound and 285 cm^{-1} when bound, leading us to propose that the carboxylate attaches to TiO_2 in a bridging mode. There is likely some degree of heterogeneity in the surface binding, however, and other modes that give rise to weaker IR bands cannot be entirely ruled out.

Time-Resolved Spectroscopic Studies. *Molecular Mo_2 Complexes.* Femtosecond (fs) and nanosecond (ns) transient absorption spectra were recorded in THF solution for the three neutral complexes (see Figures S1 and S2 of the Supporting Information). The lifetimes of the S_1 MLCT states fall in the range of 6−12 ps, and the lifetimes of the T_1 states are all roughly 60 μs. These values are summarized in Table 4 and are typical for Mo_2 quadruply bonded complexes.[23]

Time-resolved infrared (TRIR) studies were also carried out for the neutral complexes **1** and **3** as well as for the salt **4**. The monothienyl complex represents the simplest situation and was used as a model case to aid in assignment of the excited-state vibrations. Immediately after excitation, the spectra (Figure 9) display bleaches from the ground-state vibrations: $\nu_{as}(CN_2)$ at 1540 cm^{-1}, $\nu_{as}(CO_2)$ at 1504 cm^{-1}, $\nu_s(CN_2)$ at 1445 cm^{-1}, and $\nu_s(CO_2)$ at 1390 cm^{-1}. Also apparent are broad transient

Table 4. ^{1}MLCT and ^{3}MoMo$\delta\delta^*$ Lifetimes for *cis*-$Mo_2(DAniF)_2(L)_2$ Complexes 1−4

	τ (^{1}MLCT) (ps)	τ (^{3}MoMo$\delta\delta^*$) (μs)
1	6.7 ± 1.1	63.4 ± 0.8
2	6.2 ± 0.3	69.1 ± 3.3
3	11.2 ± 0.1	58.1 ± 0.4
4	18.2 ± 1.0[a]	

[a]Obtained from fs TRIR data.

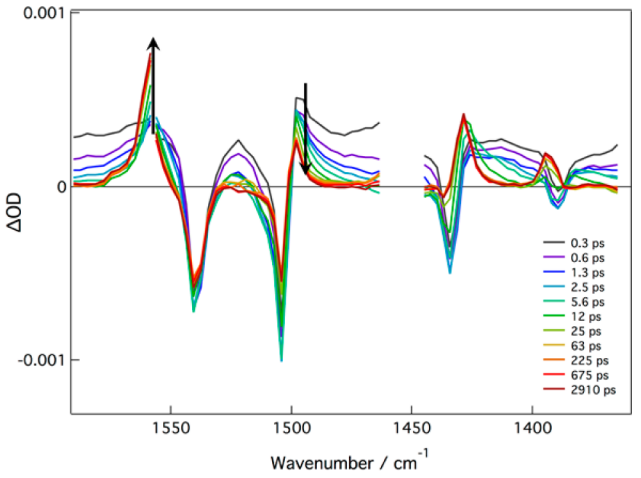

Figure 9. fs TRIR spectra of complex **1** collected in THF at room temperature, with λ_{ex} = 400 nm.

features for the ^{1}MLCT state, with an evident peak because of $\nu_{as}(CO_2)$ shifted to lower energy from the ground state by ~6 cm^{-1}. No other well-defined peaks are observed, but as the S_1 state decays to form the ^{3}MoMo$\delta\delta^*$ T_1 state, a $\nu_{as}(CN_2)$ band grows at 1558 cm^{-1} and $\nu_{as}(CO_2)$ remains present at 1498 cm^{-1}. The shift of the formamidinate vibrations to higher energy in the triplet state is due to removal of an electron from the Mo_2 δ orbital, which is involved in backbonding to the NCN π^* orbital. Although this would conceivably also reduce backbonding to the carboxylate group, there is likely a combination of influences, including enhanced donation from the formamidinate groups, that causes the slight shift to lower energy observed for $\nu_{as}(CO_2)$. This trend is predicted by DFT calculations performed on the T_1 state and was seen for previously studied Mo_2 complexes containing amidinate and carboxylate ligands.[26]

The TRIR spectra associated with complex **3** are shown in Figure 10. In the ^{1}MLCT state, $\nu_{as}(CO_2)$ is shifted 6 cm^{-1} to lower energy from the ground state, similar to complex **1**. The most striking difference for this compound is the appearance of an intense band in the singlet state at 1550 cm^{-1} that initially grows, blue shifts within the first 2 ps, and then decays with the singlet lifetime of 12 ps. Because this band displays a cooling component and is unobserved in the monothienyl complex, it is ascribed to a thiophene ring C═C vibration in the photo-excited quinoidal-type structure of the terthienyl carboxylate.[34] At long times (>200 ps), vibrational features of the MoMo$\delta\delta^*$ triplet state are observed that are almost identical to those for complex **1** above.

Spectra were also collected on complex **4** containing terminal carboxylate groups (Figure 11a). The spectra are largely similar to the neutral terthienyl complex, with singlet features at 1550 and 1495 cm^{-1}. The singlet lifetime is extended to 18 ps, and

dx.doi.org/10.1021/ja504944d | J. Am. Chem. Soc. 2014, 136, 11428−11435

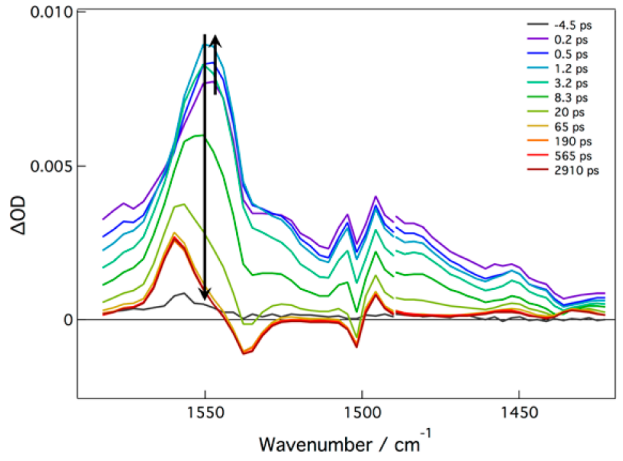

Figure 10. fs TRIR spectra of complex **3** collected in THF at room temperature, with λ_{ex} = 550 nm.

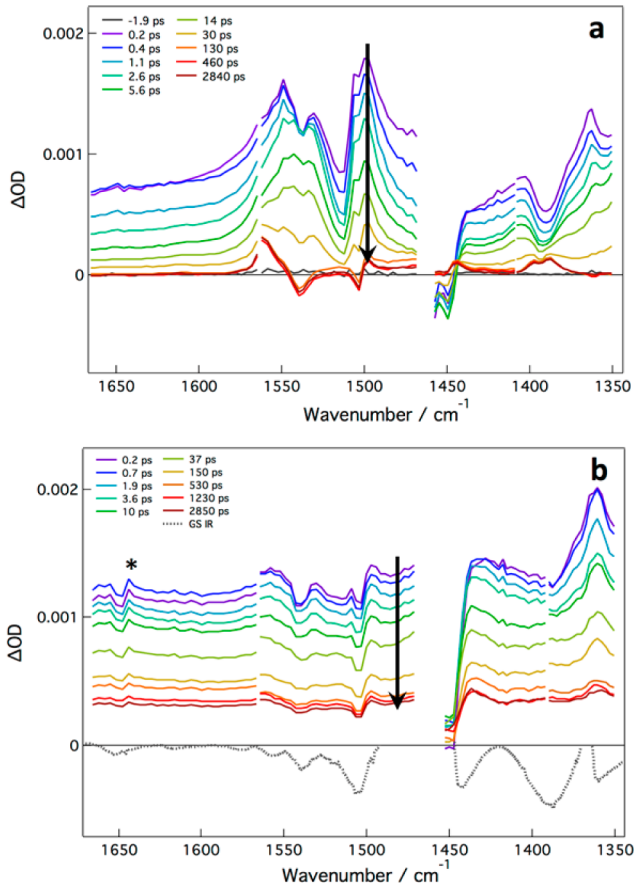

Figure 11. fs TRIR spectra of (a) complex **4** and (b) suspension of Mo_2@TiO_2 collected in THF at room temperature, with λ_{ex} = 600 nm. The asterisk denotes $\nu_{as}(CO_2')$ in the charge separated state.

following this decay, the typical vibrations for a ^{3}MoMo$\delta\delta$* state are present for the remainder of the experiment. Somewhat interestingly, no evidence of the terminal carboxylate vibration, $\nu(CO_2')$, near 1610 cm^{-1} is observed. This suggests that there is little change in the electron density of this group in the singlet and triplet excited states relative to the ground state.

Mo_2@TiO_2. The TRIR experiment was subsequently performed on a suspension of Mo_2@TiO_2 in THF (Figure 11b). A notable difference in these spectra as compared to Figure 11 is the appearance of a very broad absorption covering the entire wavenumber region. This mid-IR absorption is attributed to electrons in the conduction band or intraband gap trap states of TiO_2 and is taken as evidence of photoinduced electron transfer from the adsorbate to the semiconductor.[12,35,36] Oxidation of the Mo_2 center can be monitored simultaneously by collecting spectra in the lower energy region, where ligand vibrations occur. On top of the broad absorption, we observe ground-state bleaches of $\nu_{as}(CN_2)$ and $\nu_{as}(CO_2)$ at 1540 and 1505 cm^{-1} and weak transient peaks that correlate to those of a $(Mo_2^+)N_2O_2$ center, as predicted by DFT calculations (see Table S1 of the Supporting Information). There is also a bleach from the TiO_2-bound carboxylate vibration $\nu(CO_2')$ at 1650 cm^{-1} which was not seen for the free complex, and the frequency shifts roughly 5 cm^{-1} to lower energy after photoexcitation. Taken together, these features are indicative of electron transfer from the unrelaxed ^{1}MLCT state of the Mo_2 complex to TiO_2 within the time resolution of the experiment (<100 fs).

In previous studies using ruthenium dyes, kinetics of the mid-IR absorption band reveal multiexponential electron injection with an ultrafast (<100 fs) component from the unrelaxed excited state and a slower component from the ^{3}MLCT state that ranges from 1 to 500 ps depending upon the experimental conditions.[12,15] Decay of the band because of back electron transfer (BET) typically occurs on a micro- or millisecond time scale; however, shorter decay components are also present, with lifetimes ranging from 100 ps to 10 ns.[36,37] The dynamics observed for Mo_2@TiO_2 are somewhat different in that only a decrease of the signal occurs, which can be fit to a triple exponential with decay constants of 5 ps (0.41), 50 ps (0.45), and ~600 ps (0.14) (see Figure S3 of the Supporting Information). There is also a fourth component that is unresolvable on the time scale of the experiment and can only be estimated as >3 ns. Because electron transfer is not expected to be completely efficient,[16] some complex will remain in its unoxidized form and τ_1 may result from a reduced ^{1}MLCT lifetime of the bound species. The τ_2 and τ_3 decay constants could be assigned to rapid BET or trapping/cooling of the injected electron in the conduction band.

It has been previously observed that, when an electron is transferred to TiO_2 from an energy significantly above the conduction band edge, cooling of the "hot" electron leads to a decrease in the IR absorption cross-section and reduces the observed signal. This was explored in detail by Lian et al. with a series of $Re(CO)_3$(dcbpy) complexes bound to TiO_2.[13,38] When slow injection was inhibited, the electron absorption decayed with time constants of ~90 ps and ≫1 ns, where the faster component was attributed to electron relaxation. In the present case, excitation of the Mo_2 complex produces a Franck–Condon state that lies 1.3 eV above the conduction band edge and electrons are injected from this "hot" state. It is therefore reasonable that cooling within the conduction band is responsible for the τ_2 decay component. Both τ_3 and τ_4 may be assigned to BET. Similar non-exponential behavior has been observed for porphyrin dyes and was assigned to electrons present in a distribution of trap states, with recombination from shallow traps occurring faster than that from deep traps.[39−42]

In the spectra at long times in Figure 11b, signatures of $\nu(CN_2)$ and $\nu(CO_2)$ remain discernible on top of the broad band because of an oxidized Mo_2 center, although they are likely superimposed with those of a populated ^{3}MoMo$\delta\delta$*

dx.doi.org/10.1021/ja504944d | J. Am. Chem. Soc. 2014, 136, 11428−11435

state. Evidence of the terminal carboxylate $\nu(CO_2')$ with a reduced intensity is also present. This vibration is expected to be affected by the electric field generated following charge transfer and, thus, may not be significantly altered from the ground state after electron diffusion and recombination.

Energy Level Considerations. At this point, it is worth returning to a comparison of the Mo_2 dicarboxylate and Ru(II) dcbpy-based complexes and their ability to act as photoinduced electron transfer agents to TiO_2. On the basis of electrochemical and optical spectra, we can formulate the energy diagram shown in Figure 12. Both the dimolybdenum and

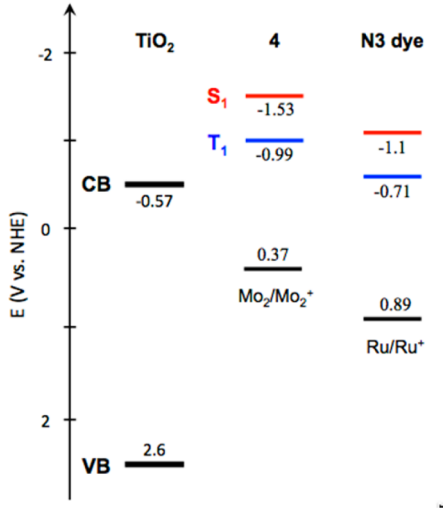

Figure 12. Energy level diagram comparing the oxidation, singlet-state, and triplet-state energies of the Mo_2 terthienyl dicarboxylate complex **4** and the Ru(II) N3 dye referenced to NHE. Positions of TiO_2 and N3 energy levels are taken from earlier studies.[12,14]

ruthenium dyes are capable of electron transfer to TiO_2 from their respective ^{1}MLCT states. For ruthenium complexes, charge injection must be very fast (<100 fs) from the short-lived S_1 state and competes with intersystem crossing (ISC).[12] The N3 ^{3}MLCT state is also above the conduction band edge and can undergo slower electron injection (1−100 ps).[12,37]

For the Mo_2 dye, the T_1 state is ^{3}MoMo$\delta\delta^*$ and lies at approximately −1 eV. Although it is energetically possible to obtain electron transfer from this triplet state, it is unlikely to be significant because it is localized on the Mo_2 center and not adjacent to the TiO_2 surface. This accounts for the lack of a growth component in the TRIR spectra (Figure 11b). The longer singlet lifetimes of these complexes should allow for sufficient time for charge injection to occur without significant interference from ISC. Additional consideration must be given to the oxidation potential of the metal center. For the *cis*-formamidinate Mo_2 complexes, oxidation occurs at 0.4 V, which is almost isoenergetic with the I^-/I_3^- redox couple typically used in dye-sensitized solar cells. The small driving force for re-reduction of the Mo_2 center may inhibit the use of these complexes in DSSC devices. However, we are able to move the oxidation to more positive potentials by replacing the formamidinate ligands with carboxylates, and studies are currently underway with dyes of this type.

CONCLUDING REMARKS

This work provides the first example of the attachment of a Mo_2^{4+}-containing photon harvester to the surface of TiO_2 nanoparticles and demonstration of its ability to undergo photoinduced electron transfer. The geometrical arrangement of the *cis*-carboxylato and *cis*-formamidinato ligands favors directed charge injection into the semiconductor in a manner akin to that of the now well-established Grätzel ruthenium polypyridyl dyes. Many aspects of the two systems are complementary, although the S_1 MLCT states of the Mo_2 complexes have lifetimes 2−3 orders of magnitude longer. Also worth noting is that molybdenum is a relatively earth-abundant and inexpensive metal in contrast to the more commonly employed d^6 and d^8 metal photon harvesters involving ruthenium, rhenium, and platinum.

Much like the Ru^{2+} dyes, the energetics of Mo_2 complexes can readily be tuned by modifying the attendant ancillary ligands, R. Particularly noteworthy is the ability to attach a $R_2Mo_2(CH_3CN)_4^{2+}$ species with two open coordination sites to nanoparticles with a dicarboxylate ligand already adsorbed to the surface. In this manner, a variety of precursors may be employed. Not only will this influence the orbital energies but it is also expected to affect the dynamics of BET from TiO_2. These are matters of continuing research.

ASSOCIATED CONTENT

Supporting Information

Materials and methods, full crystallographic information, fs and ns transient absorption spectra, and relevant kinetic traces. This material is available free of charge via the Internet at http://pubs.acs.org.

AUTHOR INFORMATION

Corresponding Authors

chisholm@chemistry.ohio-state.edu
gustafson.5@osu.edu

Notes

The authors declare no competing financial interest.

ACKNOWLEDGMENTS

The authors thank Dr. Claudia Turro for use of instrumentation and the Ohio Supercomputer Center for computational resources. This work was funded through National Science Foundation (NSF) Grants CHE-1266298 and CHE-0957191. Samantha E. Brown-Xu acknowledges support from a NSF Graduate Research Fellowship.

REFERENCES

(1) O'Regan, B.; Grätzel, M. *Nature* **1991**, *353*, 737.
(2) Hagfeldt, A.; Grätzel, M. *Acc. Chem. Res.* **2000**, *33*, 269.
(3) Grätzel, M. *Prog. Photovoltaics* **2006**, *14*, 429.
(4) Grätzel, M. *Nature* **2001**, *414*, 338.
(5) Reddy, P. Y.; Giribabu, L.; Lyness, C.; Snaith, H. J.; Vijaykumar, C.; Chandrasekharam, M.; Lakshmikantam, M.; Yum, J.-H.; Kalyanasundaram, K.; Grätzel, M.; Nazeeruddin, M. *Angew. Chem., Int. Ed.* **2007**, *46*, 373.
(6) Han, L.; Islam, A.; Chen, H.; Malapaka, C.; Chiranjeevi, B.; Zhang, S.; Yang, X.; Yanagida, M. *Energy Environ. Sci.* **2012**, *5*, 6057.
(7) Chiba, Y.; Islam, A.; Watanabe, Y.; Komiya, R.; Koide, N.; Han, L. *Jpn. J. Appl. Phys.* **2006**, *45*, L638.
(8) Grätzel, M. *Acc. Chem. Res.* **2009**, *42*, 1788.
(9) Hagfeldt, A.; Boschloo, G.; Sun, L.; Kloo, L.; Pettersson, H. *Chem. Rev.* **2010**, *110*, 6595.
(10) Yella, A.; Lee, H.-W.; Tsao, H. N.; Yi, C.; Chandiran, A. K.; Nazeeruddin, M. K.; Diau, E. W.-G.; Yeh, C.-Y.; Zakeeruddin, S. M.; Grätzel, M. *Science* **2011**, *334*, 629.

(11) Bozic-Weber, B.; Constable, E. C.; Housecroft, C. E. *Coord. Chem. Rev.* **2013**, *257*, 3089.
(12) Anderson, N. A.; Lian, T. *Annu. Rev. Phys. Chem.* **2005**, *56*, 491.
(13) Asbury, J. B.; Anderson, N. A.; Hao, E.; Ai, X.; Lian, T. *J. Phys. Chem. B* **2003**, *107*, 7376.
(14) Koops, S. E.; O'Regan, B. C.; Barnes, P. R. F.; Durrant, J. R. *J. Am. Chem. Soc.* **2009**, *131*, 4808.
(15) Juozapavicius, M.; Kaucikas, M.; van Thor, J. J.; O'Regan, B. C. *J. Phys. Chem. C* **2013**, *117*, 116.
(16) Ardo, S.; Meyer, G. J. *Chem. Soc. Rev.* **2009**, *38*, 115.
(17) Listorti, A.; O'Regan, B.; Durrant, J. R. *Chem. Mater.* **2011**, *23*, 3381.
(18) Teuscher, J.; Décoppet, J.-D.; Punzi, A.; Zakeeruddin, S. M.; Moser, J.-E.; Grätzel, M. *J. Phys. Chem. Lett.* **2012**, *3*, 3786.
(19) Alberding, B. G.; Chisholm, M. H.; Gustafson, T. L. *Inorg. Chem.* **2012**, *51*, 491.
(20) Burdzinski, G. T.; Chisholm, M. H.; Chou, P.-T.; Chou, Y.-H.; Feil, F.; Gallucci, J. C.; Ghosh, Y.; Gustafson, T. L.; Ho, M.-L.; Liu, Y.; Ramnauth, R.; Turro, C. *Proc. Natl. Acad. Sci. U. S. A.* **2008**, *105*, 15247.
(21) Chisholm, M. H.; Epstein, A. J.; Gallucci, J. C.; Feil, F.; Pirkle, W. *Angew. Chem., Int. Ed.* **2005**, *44*, 6537.
(22) Alberding, B. G.; Chisholm, M. H.; Gallucci, J. C.; Ghosh, Y.; Gustafson, T. L. *Proc. Natl. Acad. Sci. U. S. A.* **2011**, *108*, 8152.
(23) Chisholm, M. H.; Gustafson, T. L.; Turro, C. *Acc. Chem. Res.* **2013**, *46*, 529.
(24) Chisholm, M. H.; Cotton, F. A.; Daniels, L. M.; Folting, K.; Huffman, J. C.; Iyer, S. S.; Lin, C.; Macintosh, A. M.; Murillo, C. A. *J. Chem. Soc., Dalton Trans.* **1999**, 1387.
(25) Cotton, F. A.; Lin, C.; Murillo, C. A. *Inorg. Chem.* **2001**, *40*, 478.
(26) Brown-Xu, S. E.; Chisholm, M. H.; Durr, C. B.; Lewis, S. A.; Spilker, T. F.; Young, P. J. *Inorg. Chem.* **2014**, *53*, 637.
(27) Cotton, F. A.; Murillo, C. A.; Walton, R. A. *Multiple Bonds between Metal Atoms*, 3rd ed.; Springer Science: Berlin, Germany, 2005.
(28) Dennington, R., II; Keith, T.; Millam, J.; Eppinnett, K.; Hovell, W. L.; Gilliland, R. *GaussView*; Semichem, Inc.: Shawnee Mission, KS, 2003.
(29) Alberding, B. G.; Chisholm, M. H.; Ghosh, Y.; Gustafson, T. L.; Liu, Y.; Turro, C. *Inorg. Chem.* **2009**, *48*, 8536.
(30) Finnie, K. S.; Bartlett, J. R.; Woolfrey, J. L. *Langmuir* **1998**, *14*, 2744.
(31) Keis, K.; Lindgren, J.; Lindquist, S.-E.; Hagfeldt, A. *Langmuir* **2000**, *16*, 4688.
(32) Shoute, L. C. T.; Loppnow, G. R. *J. Am. Chem. Soc.* **2003**, *125*, 15636.
(33) Meyer, G. J. *Inorg. Chem.* **2005**, *44*, 6852.
(34) Brown-Xu, S. E.; Chisholm, M. H.; Durr, C. B.; Gustafson, T. L.; Spilker, T. F. *J. Phys. Chem. A* **2013**, *117*, 5997.
(35) Zhao, H.; Zhang, Q.; Weng, Y.-X. *J. Phys. Chem. C* **2007**, *111*, 3762.
(36) Asbury, J. B.; Ellingson, R. J.; Ghosh, H. N.; Ferrere, S.; Nozik, A. J.; Lian, T. *J. Phys. Chem. B* **1999**, *103*, 3110.
(37) Kallioinen, J.; Benkö, G.; Sundström, V.; Korppi-Tommola, J. E. I.; Yartsev, A. P. *J. Phys. Chem. B* **2002**, *106*, 4396.
(38) Asbury, J. B.; Hao, E.; Wang, Y.; Lian, T. *J. Phys. Chem. B* **2000**, *104*, 11957.
(39) Weng, Y.-X.; Wang, Y.-Q.; Asbury, J. B.; Ghosh, H. N.; Lian, T. *J. Phys. Chem. B* **2000**, *104*, 93.
(40) Haque, S. A.; Tachibana, Y.; Willis, R. L.; Moser, J. E.; Grätzel, M.; Klug, D. R.; Durrant, J. R. *J. Phys. Chem. B* **2000**, *104*, 538.
(41) Gobeze, H. B.; Das, S. K.; D'Souza, F. *J. Phys. Chem. C* **2014**, DOI: 10.1021/jp412646j.
(42) Imahori, H.; Kang, S.; Hayashi, H.; Haruta, M.; Kurata, H.; Isoda, S.; Canton, S. E.; Infahsaeng, Y.; Kathiravan, A.; Pascher, T.; Chábera, P.; Yartsev, A.; Sundström, V. *Phys. Chem. A* **2011**, *115*, 3679.